Detection of CI line emission towards the oxygen-rich AGB star omi Ceti

(article starts on next page)

Astronomy & Astrophysics

LETTER TO THE EDITOR

Detection of CI line emission towards the oxygen-rich AGB star omi Ceti

M. Saberi[1], W. H. T. Vlemmings[1], E. De Beck[1], R. Montez[2], and S. Ramstedt[3]

[1] Dept. of Space, Earth and Environment, Chalmers University of Technology, Onsala Space Observatory, 43992 Onsala, Sweden
e-mail: maryam.saberi@chalmers.se
[2] Smithsonian Astrophysical Observatory, Cambridge, MA 02138, USA
[3] Department of Physics and Astronomy, Uppsala University, Box 516, 75120, Uppsala, Sweden

ABSTRACT

We present the detection of neutral atomic carbon CI($^3P_1$–$^3P_0$) line emission towards omi Cet. This is the first time that CI is detected in the envelope around an oxygen-rich M-type asymptotic giant branch (AGB) star. We also confirm the previously tentative CI detection around V Hya, a carbon-rich AGB star. As one of the main photodissociation products of parent species in the circumstellar envelope (CSE) around evolved stars, CI can be used to trace sources of ultraviolet (UV) radiation in CSEs. The observed flux density towards omi Cet can be reproduced by a shell with a peak atomic fractional abundance of 2.4×10^{-5} predicted based on a simple chemical model where CO is dissociated by the interstellar radiation field. However, the CI emission is shifted by ~4 km s^{-1} from the stellar velocity. Based on this velocity shift, we suggest that the detected CI emission towards omi Cet potentially arises from a compact region near its hot binary companion. The velocity shift could, therefore, be the result of the orbital velocity of the binary companion around omi Cet. In this case, the CI column density is estimated to be 1.1×10^{19} cm^{-2}. This would imply that strong UV radiation from the companion and/or accretion of matter between two stars is most likely the origin of the CI enhancement. However, this hypothesis can be confirmed by high-angular resolution observations.

Key words. astrochemistry – stars: individual: omi Cet, V Hya – circumstellar matter – atomic processes – stars: abundances – stars: AGB and post-AGB

1. Introduction

Low- to intermediate-mass stars lose a substantial amount of their mass through strong winds during the asymptotic giant branch (AGB) phases of stellar evolution. As a consequence, a large circumstellar envelope (CSE) containing gas and dust will form around the star (Habing 1996). These large CSEs around evolved stars provide a unique laboratory to study the late stellar evolutionary phases.

Destruction of carbon-bearing molecules by either ultraviolet (UV) photo-dissociation or shock-dissociation leads to the possible presence of CI in these CSEs (e.g. Glassgold & Huggins 1986). An enhancement of the CI line emission from these environments can, therefore, probe UV- and shock-induced chemistry.

Previous studies show the CI/CO ratio increases significantly as an AGB star evolves to the post-AGB and planetary nebula phases, suggesting an evolutionary sequence for the CI/CO ratio (e.g. Bachiller et al. 1994; Young 1997; Knapp et al. 2000). These studies suggested that CI initially forms by UV photodissociation of C-bearing molecules due to the interstellar radiation field (ISRF) when the star is at the onset of the AGB. At the end of the stellar evolution, the ratio increases significantly due to the additional photodissociation in the inner envelope by the hot central star in the post-AGB and planetary nebula phases (e.g. Knapp et al. 2000).

To date, CI has been observed around several planetary nebulae which still contain part of their envelopes. CI detections are also reported for four post-AGB stars (Knapp et al. 2000, and references therein) and C-type AGB stars IRC+10216 (Keene et al. 1993; van der Veen et al. 1998), R Scl (Olofsson et al. 2015) and (tentatively) V Hya (Knapp et al. 2000). For the AGB stars IRC+10216 and R Scl, CI appears in shells, implying that the ISRF is the main source of CI formation.

Although penetration of UV radiation from the ISRF has been considered as the main source of UV radiation in CSEs around AGB stars, there is ample evidence for the presence of internal UV radiation in the CSEs. The internal UV radiation can be generated by a hot binary companion, accretion of matter between two stars, and stellar chromospheric activity (e.g. Sahai et al. 2008; Linsky 2017). Recent Galaxy Evolution Explorer (GALEX) observations revealed 180 AGB stars (57% of the observed sample) with detectable Far- and/or Near-UV emissions (Montez et al. 2017), proving the presence of the internal UV radiation.

To address the effects of both internal and external UV radiation sources, observations of the main photodissociation/photoionization products from the most abundant species such as CO are required. Chemical models of CSEs that consider both an internal and an external UV radiation field predict the enhancement of CI and/or CII in the inner CSE (Saberi et al. in prep.). The radial distribution and the peak abundance of CI and CII mostly depend on the strength of the UV field and the H$_2$ density in the CSE. Observations of CI and CII in AGB stars with strong UV detection will help to further constrain the chemical modelling.

2. Sources

2.1. omi Cet

omi Cet belongs to the closest symbiotic binary system, the Mira AB system, which is reported to be at a distance of 92 pc (van Leeuwen 2007). The primary star omi Cet (Mira A) is an M-type AGB star with mass loss of $2.5 \times 10^{-7}~M_\odot$ yr^{-1} (Ryde & Schöier 2001, hereafter RS01), and the companion, VZ Cet (Mira B) is believed to be a white dwarf (Sokoloski & Bildsten 2010). Previous imaging of the Mira AB system has shown that the circumstellar material of omi Cet is flowing towards the companion (Karovska et al. 1997, 2005). Moreover, Ramstedt et al. (2014) observed a bubble-like structure in the south-east part of the Mira AB system in CO(3–2) line emission. They suggested that it is formed due to blowing of the circumstellar material of omi Cet by the wind of the companion (Mira B). They also show that the CO emission is very extended ($\sim$20″) and arises in a range of local-standard-of-rest (lsr) velocities 37–54 km s^{-1} which indicates a relatively low wind velocity of 5 km s^{-1}. However, this velocity is larger than the 2.5 km s^{-1} wind velocity reported by RS01.

UV emission from the Mira AB system has been studied by numerous space-based UV observatories (Cassatella et al. 1979; Stickland et al. 1982; Karovska et al. 1997; Wood et al. 2001; Wood & Karovska 2004; Martin et al. 2007). Broad band fluxes from more recent UV observations with the GALEX are reported in Montez et al. (2017).

2.2. V Hya

V Hya is a carbon-type AGB star which is believed to be in transition to the planetary nebulae phase (e.g. Knapp et al. 2000; Sahai et al. 2016). It is located at a distance of 380 pc (Perryman et al. 1997) and has a mass loss rate of $1.5 \times 10^{-6}~M_\odot$ yr^{-1} (Knapp et al. 2000). Sahai et al. (2016) reported a high-speed ($\sim$200–250 km s^{-1}) ejection of the circumstellar material around V Hya every $\sim$8.5 yr which is associated with the periastron passage of a binary companion in an eccentric orbit. The first detection of V Hya in the UV was made with IUE (Barnbaum et al. 1995). V Hya was subsequently observed and detected multiple times with GALEX (Sahai et al. 2008; Montez et al. 2017).

3. Observations

The observations of the ground-state fine structure of the CI($^3P_1$–$^3P_0$) line at 492.16 GHz were performed with the Swedish Heterodyne Facility Instrument (SHeFI; Vassilev et al. 2008; Belitsky et al. 2006) on the APEX[1] 12-meter telescope (Güsten et al. 2006) located on Llano Chajnantor in northern Chile in Aug 2017 (project ID: O-0100.F-9317A-2017). Instrument specifics are listed in Table 1.

The measured antenna temperatures are converted to the main-beam temperature using $T_{\rm mb} = T^*_{\rm A}/\eta_{\rm mb}$. We used the GILDAS/CLASS[2] package to reduce the data. A first-order polynomial baseline was subtracted from the averaged spectra. The uncertainty on the absolute intensity scale is estimated to be 20%. Total integration times (on+off) are 240 min and 65 min for omi Cet and V Hya, respectively.

Table 1. Frequency, main beam efficiency, $\eta_{\rm mb}$, half power beam width, $\theta_{\rm mb}$, and the excitation energy of the upper transition level, $E_{\rm up}$.

Trans.	Tel.	Freq. [GHz]	$\eta_{\rm mb}$	$\theta_{\rm mb}$ [″]	$E_{\rm up}$ [K]
CI(1–0)	APEX	492.16	0.60	12.67	23.62

Table 2. CI observational results for omi Cet.

Star	$V_{\rm LSR}$ [km s^{-1}]	$V_{\rm c}$ [km s^{-1}]	$I_{\rm CI}$ [K km s^{-1}]	$T_{\rm peak(MB)}$ [K]	ΔV [km s^{-1}]
omi Cet	47.2	43.4±0.6	0.55±0.07	0.054	9.5±1.3

Notes. The stellar velocity $V_{\rm LSR}$ was taken from Khouri et al. (2016). The central velocity, $V_{\rm c}$, velocity-integrated line intensity, $I_{\rm CI}$, the peak line temperature, $T_{\rm CI(MB)}$, and the FWHM linewidth, ΔV, were found by fitting a Gaussian line profile to the data.
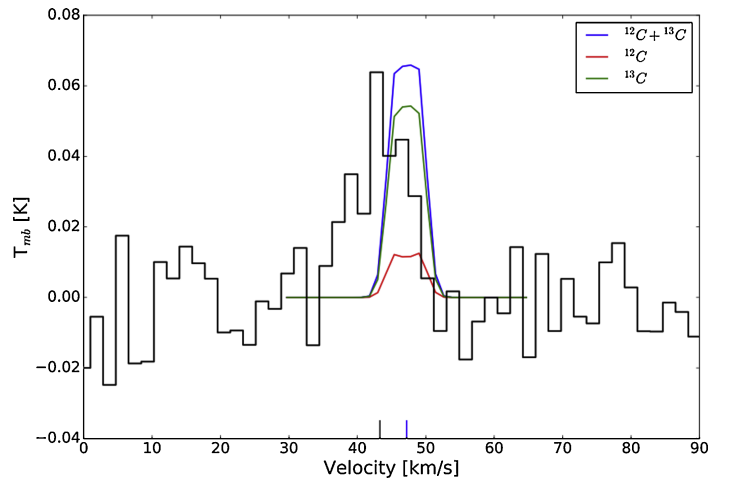

Fig. 1. CI emission towards omi Cet at 1.8 km s^{-1} velocity resolution (black). The stellar $v_{\rm LSR}$ (47.2 km s^{-1}) and the spectrum peaks $v_{\rm LSR}$ (43.4 km s^{-1}) are indicated as vertical markers on the *x*-axis in blue and black, respectively. The results of RT modelling of both ^{12}C and ^{13}C isotopes are also shown in red and green, respectively. The blue profile indicates the total amount of C.

We note that frequency shifts of the two isotope ^{13}CI($^3P_1$–$^3P_0$) hyperfine lines with respect to the frequency of the ^{12}CI($^3P_1$–$^3P_0$) line are only 0.5 MHz and 3.6 MHz for the F=1/2−1/2 and 3/2−1/2 components, respectively, indicating that we have both ^{12}C and ^{13}C contributing to the total flux.

4. Results and discussion

4.1. omi Cet

We present the spectrum of omi Cet in Fig. 1 and summarise the results in Table 2. In the following subsections we describe the radiative transfer (RT) models that we run to determine the circumstellar CI abundance.

4.1.1. The circumstellar model

To model the envelope around omi Cet, we assume a uniformly expanding spherical envelope which is formed due to a constant mass-loss. We adopt the physical properties of the CSE from CO RT modelling results obtained by RS01; see Table 3 in that paper. Using the given CSE properties, the updated CO molecular data, and the updated distance of 92 pc for omi Cet,

we could reasonably model the CO(J=2–1, 3–2, 4–3) emission lines observed by JCMT. Although the model reasonably reproduces the CO observations, it is not possible to constrain the complex outflow around omi Cet based on the single-dish observations; it is therefore a crude approximation of the CSE properties.

A non-local thermodynamic equilibrium (non-LTE) RT code based on the Monte Carlo program (MCP; see e.g. Bernes 1979; Schöier & Olofsson 2001) was used to analyse the circumstellar CI emission. The CI is assumed to be excited by collision with H_2 molecules and through radiation from the central star, the dust and the cosmic microwave background. The collisional data are taken from Schroder et al. (1991). They cover temperatures from 10 to 500 K.

To derive the CI abundance distribution through the envelope, we used an extended version of the publicly available circumstellar envelope chemical model code[3] (McElroy et al. 2013). The extended version includes ^{13}C and ^{18}O isotopes and the molecules containing these isotopes in addition to a more extended chemical network (Saberi et al., in prep.). The result of the chemical modelling is presented in the Appendix. We used the ^{12}C and ^{13}C abundance distributions that are shown in Fig. A.1 as input files in the MCP.

Results of the RT modelling for both C isotopes and the integrated flux of both isotopes are presented in Fig. 1. The flux is dominated by ^{13}CI line emission since it originates closer to the star where ^{12}CO is more efficiently self-shielded while the less abundant ^{13}CO would be dissociated in the more inner region (Lee 1984).

The model produces a narrower line profile than observed in the spectrum. The narrow width of the profile is due to the low expansion velocity 2.5 km s^{-1} of the CSE that was assumed in the RS01 model. There is also a shift (~4 km s^{-1}) between the central peak of the spectrum and the model. We cannot explain the velocity shift under the assumption of an external UV field impacting on a regular circumstellar envelope which leads a spherically symmetric CI distribution, centred around the star, and hence around the stellar v_{LSR}.

4.1.2. Constraining the CI emitting region

The observed UV fluxes towards the symbiotic binary suggest that the measured CI spectrum could arise from a more compact region near the binary companion. We combined the CO(3–2) ALMA observations from projects 2012.1.00524.S (PI: Ramstedt) and 2013.1.00047.S (PI: Planesas) to reach an angular resolution of 0.28″. We show the CO(3–2) line emission map at v_{LSR} = 43.3 km s^{-1}, the closest to the CI peak velocity, in Fig. 2. As shown, there are three components that peak around Mira A, Mira B, and the north part of the Mira AB system in the CO(3–2) emission. If the total CI flux was coming from Mira A, we would not expect to observe such a velocity shift between the CI peak emission and the stellar velocity as we discussed in the Sect. 4.1.1. There are no known sources of UV- or shock-dissociation near the clump in the north part that cause the enhancement of the CI emission. Therefore, the most likely hypothesis is that CI arises from the component near Mira B due to the strong UV emission. The velocity shift could then be the result of the orbital velocity of Mira B around Mira A. Although the orbital velocity of Mira B is not yet accurately known, based on the orbital parameters (Prieur et al. 2002) it is of the order of 6 km s^{-1}.
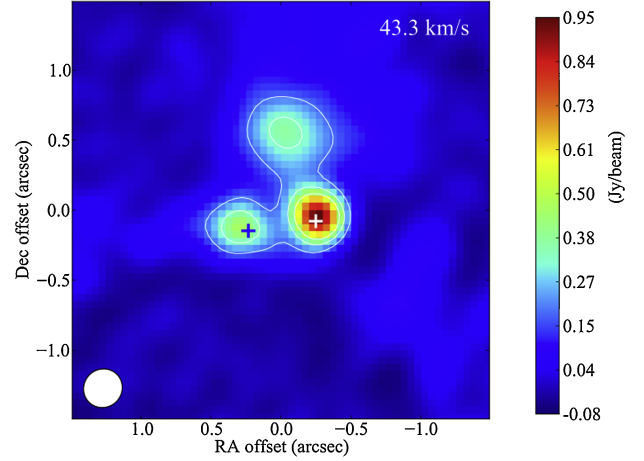
---
3 http://udfa.ajmarkwick.net/index.php?mode=downloads

Fig. 2. ALMA observations of CO(3–2) towards the Mira AB system at v_{lsr} = 43.3 km s^{-1}. The white and blue plus symbols show the positions of omi Cet (Mira A) and VZ Cet (Mira B), respectively. The contours are overlaid on the image with 20, 35, and 50% of the peak value. The observed CI emission likely arises from the region near Mira B. The beam is shown in the lower left corner.

4.1.3. The CI abundance in the postulated emitting region

We derive the CI abundance assuming it comes from the component around Mira B seen in Fig. 2. This component has a radius ~0.2″ = 2.67 ×10^{14} cm. The publicly available non-LTE RT code RADEX[4] is used to model the CI emission.

The input parameters used in RADEX are listed in Table 3. The H_2 number density is calculated assuming a constant mass-loss rate and constant expansion velocity as in Schöier & Olofsson (2001). We assumed the temperature profile $T(r) = 150 (10^{15}/r)$ as given by RS01. Here we assumed the updated distance 92 pc reported by van Leeuwen (2007) since using the correct distance is crucial in calculating the column density. We consider constant H_2 number density and kinetic temperature profiles in the constrained region. These are calculated at the Mira B position r = 60 AU = 8.97 ×10^{14} cm from omi Cet. The line width is estimated by fitting a Gaussian profile to the observed spectrum. The only free parameter in this modelling is the CI column density.

In RADEX, the calculated radiation temperature of the spectral line T_R is equivalent to the main beam antenna temperature divided by the dilution factor for an unresolved source. With a telescope beam size of ~13″ and assuming an emission region of 0.4″, we get a dilution factor of $(0.4/13)^2 \sim 0.001$. This leads to a corrected main beam temperature of 0.054/0.001 = 54 K. To reproduce this temperature, a CI column density of 1.1×10^{19} cm^{-2} is needed for the component near to Mira B. We note that the radiation temperature T_R is not very sensitive to the H_2 density and the kinetic temperature. T_R does not change more than 10% over ranges of $1 \times 10^6 < n_{H_2} < 1 \times 10^{12}$ cm^{-3} and $100 < T_{kin} < 500$ K.

The CI/H_2 ratio strongly depends on the true size and the H_2 number density of the emitting region. Since the circumstellar material of omi Cet is accreted onto and heated by the binary companion, we would expect a higher H_2 density and temperature in the clump compared to the values that were derived from the smooth wind model. Ireland et al. (2007) infer an overdensity around Mira B of a factor of 25–100 compared to the smooth wind model. If we assume the H_2 density is 1.9×10^8 cm^{-3} in the

---
4 http://var.sron.nl/radex/radex.php

Table 3. Input parameters used in RADEX to determine the CI abundance towards omi Cet.

$T_{back.}$	T_{Kin}	H$_2$ density	Line width	CI column density
[K]	[K]	[cm^{-3}]	[km s^{-1}]	[cm^{-2}]
2.73	170	1.9E6	9.5	1.1E19

clump (higher by a factor of 100 compared to the smooth wind model), then our measurement implies a fractional abundance CI/H$_2 \sim 1.1 \times 10^{-4}$ in this location. However, to accurately determine the CI/H$_2$ ratio we need to constrain the true size of the emitting region, requiring high-angular-resolution observations of the CI line emission. Additionally, high-angular-resolution observations of multiple transitions of a collisionally excited molecule like CO would allow a better H$_2$ density estimate in the CI-emitting region.

4.1.4. The CI/CO ratio

To derive the CI/CO ratio, we need to know the size and the H$_2$ density of the emitting region. Assuming the smooth wind model without enhancement of the H$_2$ density in the clump and the abundance ratio CO/H$_2 \sim 5 \times 10^{-4}$ (RS01), we derive a CI/CO $\sim$ 20 which is unrealistically high. If we assume the enhancement of H$_2$ density by a factor of 100 as was explained in Sect. 4.1.3, we find a ratio CI/CO $\sim$ 0.2. This ratio is similar to the CI/CO $\sim$ 0.2–0.5 reported in the detached-shell of R Scl (Olofsson et al. 2015) and the ratio of ~0.3 reported for V Hya (Knapp et al. 2000), and higher than the ratio ~0.02 reported for IRC+10216 (Young 1997).

It is worth mentioning that a strong detection of CI was reported in the inner part of the O-rich supergiant star α Ori (Betelgeuse) (Huggins et al. 1994; van der Veen et al. 1998). These authors interpret the high observed ratio of CI/CO $\sim$ 5 as being due to the presence of a chromosphere and therefore extra UV radiation. Similarly, the CI emission towards omi Cet likely arises from the inner region near its binary companion, showing the extra UV-dissociation in the inner CSE around the companion of an AGB star.

4.2. V Hya

The observed spectrum towards V Hya is presented and discussed in the Appendix (Fig. A.2). Our detection of CI for V Hya is consistent with the previous detection reported by Knapp et al. (2000).

5. Conclusion

In this letter, we report the CI line emissions from omi Cet (M-type) and V Hya (C-type) AGB stars. omi Cet is the first O-rich AGB star with a CI detection. The CI column density of omi Cet is estimated to be ~1.1 $\times 10^{19}$ cm^{-2} if the emission arises from a compact region near the hot secondary star, Mira B. In that case, the UV emission from Mira B and/or from the accretion of matter from the wind of Mira A onto Mira B is the likely cause for the observed CI enhancement. On the other hand, the observed flux is consistent with CI in a shell produced by CO dissociation from the ISRF. However this model does not correctly explain the observed line width and the velocity shift between the peak of CI emission and the stellar velocity. Since there could be other kinematic effects in such a complex envelope however, we cannot confidently rule out the external UV field. Only higher-angular-resolution maps will be able to

determine the real CI distribution and thus the origin of the CI enhancement.

Definite detections of CI were previously reported in IRC+10216 and R Scl, two carbon-rich AGB stars. Our observations bring the number of CI detection of AGB stars to four in total and the number of evolved stars (including transition objects) to nine (Knapp et al. 2000, and references therein).

The spatial abundance distribution of circumstellar products of photodissociation and ionisation can provide insight into the relevant sources of UV radiation, by probing the effects of (unidentified) hot binary companions and stellar chromospheric activity of AGB stars.

References

Bachiller, R., Huggins, P. J., Cox, P., & Forveille, T. 1994, A&A, 281, L93
Barnbaum, C., Morris, M., & Kahane, C. 1995, ApJ, 450, 862
Belitsky, V., Lapkin, I., Monje, R., et al. 2006, in SPIE Conf. Ser., Proc. SPIE, 6275, 62750G
Bernes, C. 1979, A&A, 73, 67
Cassatella, A., Gura, D., Reimers, D., & Stickland, D. 1979, IAU Circ., 3425
Glassgold, A. E. & Huggins, P. J. 1986, ApJ, 306, 605
Güsten, R., Nyman, L. Å., Schilke, P., et al. 2006, A&A, 454, L13
Habing, H. J. 1996, A&ARv, 7, 97
Hinkle, K. H., Lebzelter, T., & Straniero, O. 2016, ApJ, 825, 38
Huggins, P. J., Bachiller, R., Cox, P., & Forveille, T. 1994, ApJ, 424, L127
Ireland, M. J., Monnier, J. D., Tuthill, P. G., et al. 2007, ApJ, 662, 651
Karovska, M., Hack, W., Raymond, J., & Guinan, E. 1997, ApJ, 482, L175
Karovska, M., Schlegel, E., Hack, W., Raymond, J. C., & Wood, B. E. 2005, ApJ, 623, L137
Keene, J., Young, K., Phillips, T. G., Buettgenbach, T. H., & Carlstrom, J. E. 1993, ApJ, 415, L131
Khouri, T., Vlemmings, W. H. T., Ramstedt, S., et al. 2016, MNRAS, 463, L74
Knapp, G. R., Jorissen, A., & Young, K. 1997, A&A, 326, 318
Knapp, G. R., Crosas, M., Young, K., & Ivezić, Ž. 2000, ApJ, 534, 324
Lee, L. C. 1984, ApJ, 282, 172
Linsky, J. L. 2017, ARA&A, 55, 159
Martin, D. C., Seibert, M., Neill, J. D., et al. 2007, Nature, 448, 780
McElroy, D., Walsh, C., Markwick, A. J., et al. 2013, A&A, 550, A36
Montez, Jr. R., Ramstedt, S., Kastner, J. H., Vlemmings, W., & Sanchez, E. 2017, ApJ, 841, 33
Olofsson, H., Bergman, P., & Lindqvist, M. 2015, A&A, 582, A102
Perryman, M. A. C., Lindegren, L., Kovalevsky, J., et al. 1997, A&A, 323, L49
Prieur, J. L., Aristidi, E., Lopez, B., et al. 2002, ApJS, 139, 249
Ramstedt, S., Mohamed, S., Vlemmings, W. H. T., et al. 2014, A&A, 570, L14
Ryde, N. & Schöier, F. L. 2001, ApJ, 547, 384
Sahai, R., Findeisen, K., Gil de Paz, A., & Sánchez Contreras, C. 2008, ApJ, 689, 1274
Sahai, R., Scibelli, S., & Morris, M. R. 2016, ApJ, 827, 92
Sarre, P. J., Hurst, M. E., & Lloyd Evans, T. 2000, MNRAS, 319, 103
Schöier, F. L., & Olofsson, H. 2001, A&A, 368, 969
Schöier, F. L., Ramstedt, S., Olofsson, H., et al. 2013, A&A, 550, A78
Schroder, K., Staemmler, V., Smith, M. D., Flower, D. R., & Jaquet, R. 1991, J. Phys. B At. Mol. Phys., 24, 2487
Sokoloski, J. L., & Bildsten, L. 2010, ApJ, 723, 1188
Stickland, D. J., Cassatella, A., & Ponz, D. 1982, MNRAS, 199, 1113
van der Veen, W. E. C. J., Huggins, P. J., & Matthews, H. E. 1998, ApJ, 505, 749
van Leeuwen, F. 2007, A&A, 474, 653
Vassilev, V., Meledin, D., Lapkin, I., et al. 2008, A&A, 490, 1157
Wood, B. E., & Karovska, M. 2004, ApJ, 601, 502
Wood, B. E., Karovska, M., & Hack, W. 2001, ApJ, 556, L51
Wyrowski, F., Schilke, P., Thorwirth, S., Menten, K. M., & Winnewisser, G. 2003, ApJ, 586, 344
Young, K. 1997, ApJ, 488, L157

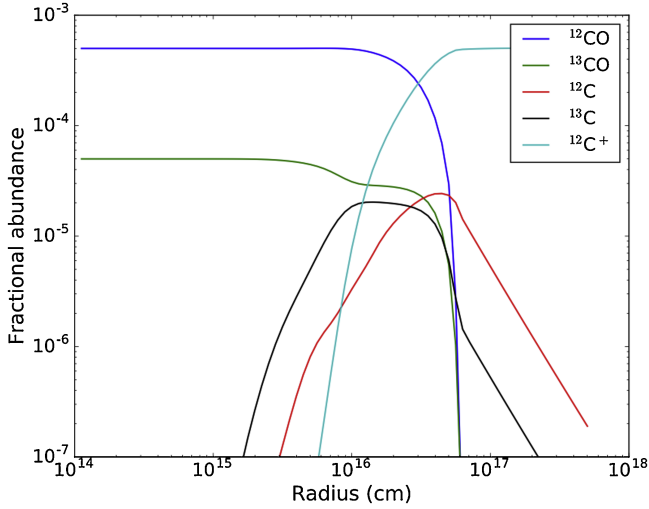## Appendix A: Chemical modelling results

Fig. A.1. The fractional abundance distribution of the circumstellar species of the Omi Cet.

Here we present the results of the chemical modelling of omi Cet. The code assumes a spherically symmetric envelope which is formed due to a constant mass-loss rate $2.5 \times 10^{-7}\ M_\odot\ \mathrm{yr}^{-1}$. The envelop expands with a constant expansion velocity $2.5\ \mathrm{km\ s}^{-1}$. The ISRF is the only UV radiation field which penetrates through the envelope from the outside. We adopt the stellar luminosity and the temperature profile of the CSE from RS01 model. We assumed the initial fractional abundances of $^{12}CO/H_2 = 5 \times 10^{-4}$ reported for omi Cet (RS01), the $^{13}CO/H_2 = 5 \times 10^{-5}$ based on the isotopic ratio reported by Hinkle et al. (2016), and the $H^{12}CN/H_2 = 1 \times 10^{-7}$ which is the average ratio reported for M-type AGB stars (Schöier et al. 2013). We do not expect a significant contribution of other C-bearing molecules for an M-type AGB star in the model. Figure A.1 shows the fractional abundance distribution of some circumstellar species through the envelope. We use the ^{12}C and ^{13}C distribution profiles as the input in our RT model.

Appendix B: V Hya spectrum

Figure A.2 shows the observed spectrum of V Hya. Although our detection of CI for V Hya is consistent with the previous detection reported by Knapp et al. (2000), the CI line emission could potentially be contaminated by HC_3N ($\nu_7=1$) vibrationally excited emission. The vibrationally excited HC_3N has been detected for the proto-planetary nebula CRL618 by Wyrowski et al. (2003). A detection of circumstellar HC_3N ground state emissions around V Hya was previously reported by Knapp et al. (1997). In addition, preliminary chemical modelling results show a large enhancement of HC_3N in the inner CSE by the internal UV radiation (Saberi et al., in prep.).

As shown in Fig. A.2, we potentially identify detection of several $SiC_2(\nu = 0)$ emission lines in the V Hya spectrum. Sarre et al. (2000) have presented the SiC_2 absorption bands in the upper atmosphere of V Hya. We cannot differentiate the possible contributions of different lines because of the low resolution of the spectrum. Therefore, we did not analyse the V Hya spectrum any further.
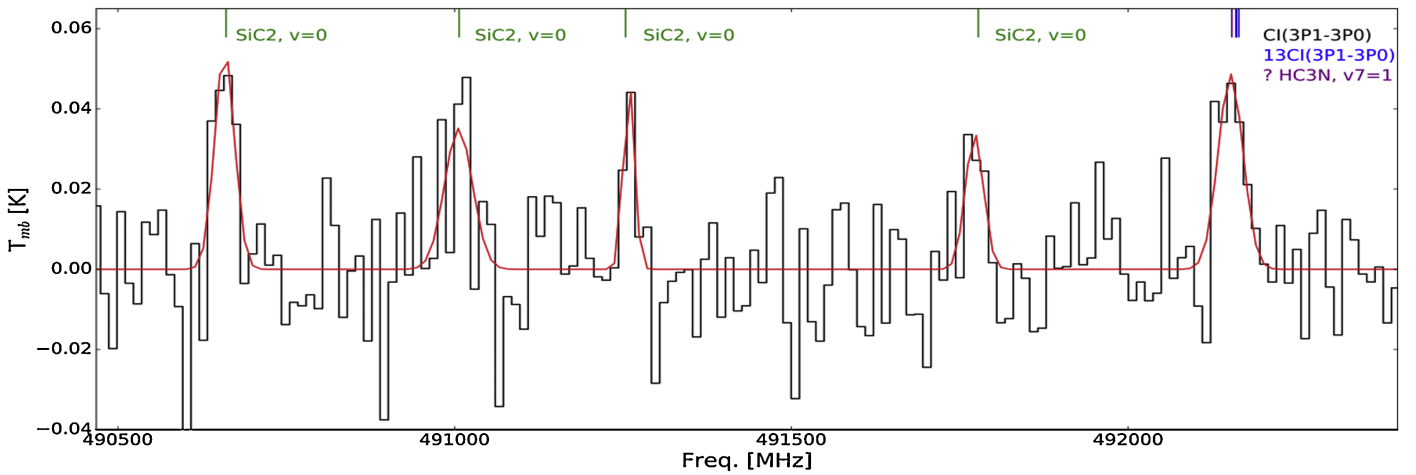

Fig. A.2. APEX observations towards V Hya at $v_{lsr} = -17\ \mathrm{km\ s}^{-1}$ with the spectral resolution 12.21 MHz (7.4 km s^{-1}) (black). The red line indicates a Gaussian fit to potential line detections.